Renewable Energy Integration in Zonal Markets

Ignacio Aravena, *Student, IEEE,* and Anthony Papavasiliou, *Member, IEEE*

***Abstract*—In this paper we investigate the impact of zonal network management in the operation of power systems with significant levels of renewable energy integration. Our study is inspired by the current state of the European energy market, and we focus on a case study of the Central Western European (CWE) system. First, we present a hierarchy of models that account for unit commitment, the separation of energy and reserves, and the simplified representation of transmission constraints in a zonal market, in order to examine the impact of these factors on efficiency in a regime of large-scale renewable energy integration. Second, we simulate operations of the CWE system under the zonal market design using a detailed instance that consists of 656 thermal generators, 679 nodes and 1073 lines, with multi-area renewable energy production and 15-minute time resolution. Zonal market operations are compared against deterministic and stochastic unit commitment using high performance computing in order to tackle the scale of the resulting models. We find that market design can have an influence on cost efficiency which far exceeds the benefits of stochastic unit commitment relative to deterministic unit commitment. We conduct a detailed analysis of the numerical results in order to explain the relative performance of the different models.**

I. Introduction

EUROPE has adhered to an ambitious renewable energy integration agenda as a key pillar of its energy and climate objectives. Over the past 5 years, the growth of renewable capacity has been especially significant in the CWE system (comprising Austria, Belgium, France, Germany, Luxembourg, the Netherlands and Switzerland). Approximately 40 GW of solar photovoltaic (PV) panels and 17 GW of wind turbines have been installed in the system between 2008 and 2013 [1]. This trend is expected to continue at the same pace towards meeting the 2020 European Union (EU) emissions targets [2]. Even further development is expected moving forward to 2050, as a result of ambitious environmental targets set by numerous countries [3].

Renewable resources cause various complications in operations, including congestion resulting from uncontrollable fluctuations of renewable energy [4] and the need to carry adequate reserves in the system. The management of unscheduled flows has been especially challenging in Europe, as evidenced for example by the externalities of renewable power integration on neighboring networks (e.g. Poland and other zones [5]). The need for European Transmission System Operators (TSOs) to pool reserves in order to better deal with the uncertainty and variability of renewable resources has been recognized recently [6] and efforts are underway for harmonizing the definition and management of reserves in Europe. Ultimately, the introduction of renewable resources induces spatial and temporal coordination requirements on operators.

The European electricity market has favored a zonal market design, known as Market Coupling (MC) [7], over locational marginal pricing (LMP) on the basis of simplicity and liquidity. There is a long-standing debate about the relative merits of the two designs, and the implementation of the market coupling design in Europe has generated considerable controversy (see [8] and references therein for a detailed discussion). European zonal markets are characterized by three features that differentiate them substantially from centralized nodal markets in the context of renewable energy integration: (*i*) the simplified representation of transmission at the day-ahead time stage, (*ii*) the sequential clearing of reserves and energy, and (*iii*) the limited real-time coordination among zones for relieving congestion and imbalances.

Several US electricity markets, such as PJM [9], MISO [10], CAISO [11] and NYISO [12], have adopted LMP and centralized operations under a single Independent System Operator (ISO). Zonal prices continue to be used for billing loads in certain markets such as NYISO [13]. Nevertheless, in contrast to market coupling, zonal prices are computed after scheduling production with a nodal model [12], hence the use of zonal prices does not create unscheduled flows on the transmission network.

The market coupling design is, to some extent, the counterpart of bilateral market-to-market operations in US power systems. Market coupling uses uniform pricing within each *bidding zone*[1] (commonly, national markets) and clears market-to-market interchanges within the European wide day-ahead energy market, implicitly allocating transmission capacity between zones [7]. US markets use LMP within each balancing authority area [14], however market-to-market interchanges are usually arranged prior to clearing of the day-ahead market in a bilateral fashion and they must to be approved by every affected ISO [14], [15]. Approved interchanges are then considered fixed and unscheduled flows caused by them are taken into account in day-ahead market operations [11].

In addition to day-ahead market design challenges, real-time operation posses several coordination challenges in systems with multiple operators [16]. Similar coordination mechanisms are used both in market coupling and wide US interconnections. In the market coupling design, balance responsible parties are entitled to maintain their scheduled *net position*[2] in real time [17]. Likewise, in US markets each balancing authority (ISO) must maintain its area control error (a measure

Manuscript received XXX; revised XXX.

I. Aravena and A. Papavasiliou are with the Center for Operations Research and Econometrics (CORE), Université catholique de Louvain, Belgium. e-mail: ignacio.aravena@uclouvain.be, anthony.papavasiliou@uclouvain.be

[1]A bidding zone is defined as a geographical area within which market participants are able to exchange energy without allocating transmission capacity [1].

[2]The net position is the netted sum of electricity exports and imports for each market time unit in a certain bidding zone [1].

consisting of the difference between scheduled and real area net position, and the area frequency deviation) below certain established limits [18].

In this policy analysis paper we present a framework for modeling the market coupling design as currently implemented in the CWE system at an operational level. In addition, we use the proposed framework to revisit the question of the relative merits of zonal and nodal markets in the context of systems with high levels of renewable energy.

A. Literature review

The impact of the simplified representation of transmission constraints in day-ahead energy markets on operational efficiency was recognized in early work by Bjørndal and Jornsten [19] and Ehrenmann and Smeers [8], whom illustrate a number of challenges in zonal markets, including efficiency losses and the difficulties of defining zones. The authors use dispatch models in order to obtain analytical insights on systems with up to 6 nodes. Van der Weijde and Hobbs [20] introduce unit commitment in the study of zonal systems. They focus on quantifying the benefits of zonal coordination in balancing, and use a two-stage model that represents the sequencing of unit commitment and dispatch decisions. Their study is focused on a 4-node system. Recent work by Oggioni *et al.* [21], [22] further refines zonal models. In [21] the authors use generalized equilibrium models in order to study the effect of coordination among TSOs on operational efficiency. The authors use a standard 6-node network and a 15-node model of the CWE system. They estimate the welfare gains of LMP pricing over zonal pricing in the CWE system at 0.001%. The authors do not account for reserves or unit commitment in their analysis. In [22] the authors evaluate the impacts of priority dispatch of wind in Germany using a zonal model of the CWE system. Uncertainty is accounted for using a scenario-based formulation, however the authors ignore unit commitment decisions in their analysis.

Studies that focus on renewable energy integration in Europe commonly ignore zonal network management either by directly assuming a nodal market [23] or by considering a zonal transportation network without addressing congestion within zones [24]–[27]. Nevertheless, a number of studies have estimated the potential efficiency gains of LMP in Europe relative to a zonal design, in the context of renewable energy integration. Leuthold *et al.* [28] estimate the welfare gains of LMP over uniform pricing at 0.8% using a model of Germany and its neighboring countries that consists of 309 nodes. Barth *et al.* [29] study the effect of international unscheduled flows using a regional model for the entire EU. The authors use a transportation model for transmission and estimate cost savings of 0.1% of nodal relative to zonal pricing. Neuhoff *et al.* [30] estimate the operating cost savings of LMP relative to zonal pricing between $1.1\% - 3.6\%$. The authors use a single-period unit commitment model of the UCTE-STUM system (4300 nodes, 6000 lines) which is simulated for two extreme operational snapshots (no wind and maximum wind). Abrell and Kunz [31] present a framework for day-ahead and intraday operation in a receding horizon scheme, emulating the sequential operation of day-ahead and intraday markets. Abrell and Kunz study a detailed model of the German grid for which they estimate efficiency losses of zonal markets at 0.6%. The authors do not consider uncertainty, assume that all thermal generators can update their commitment in real time and include topology control as a congestion management measure in the zonal market design.

An emerging aspect that results from the large-scale integration of renewable resources is the sub-hourly ramping capacity of a system. The state of the art in renewable energy integration often employs hourly time resolution for day-ahead and real-time operations [32]–[35]. Recent work by Deane *et al.* [36] and Gangammanavar *et al.* [37] underscores the importance of sub-hourly time resolution in accurately estimating the costs of integrating renewable energy. Bakirtzis *et al.* [38] propose a receding horizon model with 5-minute resolution for simulating real-time operation under large-scale renewable energy integration. In this study we develop a hybrid model that employs hourly resolution for the commitment of units, and 15-minute resolution for dispatch. This is in line with operating practice in European markets (hourly day-ahead markets [39] and a quarterly real-time balancing mechanism [6]).

This paper contributes to the existing literature by developing a detailed model of the market coupling design and analyzing a detailed instance of the CWE region, which leads to novel insights about the performance of zonal markets in a regime of large-scale renewable energy integration. In terms of modeling, we develop a hierarchy of models for the market coupling design that includes a model for available transfer capacity computation that is guaranteed to outperform previously proposed models [30], a power exchange model that accounts for unit commitment and the treatment of non-convexities by European power exchanges, and a model that emulates the decentralized process of nominations of production and reserves after the day-ahead exchange has cleared. The latter two elements are largely absent from the current literature [20]–[22], [29]–[31]. We use the proposed hierarchy of models to compare the market coupling design to deterministic and stochastic unit commitment models (centralized nodal designs). Numerical results provide novel policy insights by demonstrating that the conjunction of zonal management and unit commitment decisions, in a regime of large-scale renewable energy integration, produces effects that deviate substantially from assumptions of fully coordinated systems.

B. Paper organization

The paper is organized as follows. Section II presents the proposed model for the market coupling design, starting from an overview and introducing a hierarchy of mathematical programs to model day-ahead and real-time operations in the subsequent subsections. Section III presents the CWE system instance used in this study and the simulation setup. Section IV compares the results of the market coupling model to the actual performance of the CWE system over the reference year of the simulation. Section V compares the performance of the various policies that were investigated and analyzes the

obtained results. Finally, section VI concludes the paper and points to directions of future research.

II. A Model of European Market Coupling

The market coupling design has become the uniform paradigm for operating the European electricity markets. Through the price coupling of regions (PCR) project, the market coupling design is now present in most countries of western, central and northern Europe [40].

From an operational point of view, market coupling consists of sequential steps that are executed or supervised by power exchanges or by system operators, with some differences among countries due to local regulatory frameworks. The steps involved in the day-ahead energy market (namely, the computation of transfer capacities and the clearing of the energy market) are nearly standardized among countries. In contrast, there is substantial diversity in the definition of reserves. The procedures governing re-dispatch and balancing and the definitions of products are often incompatible among countries. These incompatibilities have already been resolved between Germany and Switzerland, and the TSOs of Belgium, Germany and the Netherlands are currently working towards harmonizing the definition and sharing of their reserve resources [6]. Further standardization is expected in the medium term following the ENTSO-E *network codes* [17], [41]. In anticipation of this harmonization, in this paper we assume that system operators adhere to a common definition of reserve products among zones.

Following the standardization of reserve products, it is expected that bidding zones will increasingly interchange secondary and tertiary reserves as is currently the case for primary reserves[3]. As opposed to primary reserves, for which shared volumes are in the order of tens of MW, the interchange of secondary and tertiary reserves might involve large volumes of power, which would require the reservation of cross-border transmission capacity between zones, as analyzed by Gebrekiros *et al.* [43]. The reservation of transmission capacity for reserve provision is currently under debate among European regulators, hence we do not include this element in our analysis in order to focus on the status quo.

Throughout the paper, we model the transmission network using a lossless DC power flow model. We assume that all dispatch decisions (production, flows) are updated every 15 minutes, whereas commitment (on/off) decisions of thermal generators are updated on an hourly basis. Thermal generators with commitment decisions are divided into two groups: *slow* generators, whose commitment must be determined in the day-ahead time frame, and *fast* generators, whose commitment can be modified in real-time operations. Following these assumptions, we model the market coupling design as depicted in Fig. 1.

At day ahead, the TSOs compute the available transfer capacities (ATCs) between the different physically connected zones in the system, for each hour τ of the next day. Then, power exchanges collect bids from firms and clear the day-ahead energy market, modeling the exchanges between zones through a transportation network limited by the ATCs. The day-ahead energy market is cleared with hourly resolution, and it determines a net position $\Delta Q^{MC}_{a,\tau}$ for each zone a for each hour τ of the next day, as well as a preliminary commitment for slow generators $\boldsymbol{u}^{MC}$.

After the energy market clears and before firms communicate their final schedule to the corresponding TSO, firms within each zone can trade among each other their production and reserve obligations [44], [45]. We model this decentralized process as a cost minimizing scheduling that aims at meeting security targets for real-time operation. This procedure results in final commitment decisions for slow generators, $\boldsymbol{u}^{R}$, that comply with the energy balance and reserve requirements of each zone. Note that reserve obligations of firms are determined in monthly or weekly tenders, prior to day-ahead energy market clearing [6]. We assume that the forward positions of the reserve tendering process are adjusted by firms after the day-ahead exchange clears, hence we do not represent these forward auctions explicitly in our analysis.

Finally, the resolution of congestion (referred to as re-dispatch) and the resolution of imbalances due to outages and forecast errors (referred to as balancing) take place in real time on 15-minute intervals, while respecting the net position of each zone $\boldsymbol{\Delta Q}^{MC}$ [17] and the commitment of reserves $\boldsymbol{u}^{R}$. At this stage, we assume that TSOs in charge of the possibly multiple *control areas*[4] within each bidding zone fully coordinate their operations and that they net out their scheduled net positions for balancing purposes [46]. This assumption allows us to model each individual bidding zone as if it were operated by a single TSO in real time.

A. Computation of available transfer capacity

Power exchanges use the simplified transportation network presented in Fig. 2 for representing transmission constraints among zones in the CWE system. The topology of this zonal network is determined by the topology of the real network and it includes an interconnector between each pair of adjacent zones. Flows on the zonal network are limited by the ATCs, which must be computed on a daily basis by the TSOs and communicated to power exchanges.

The first step in the computation of ATCs is the determination of total transfer capacities (TTC) among zones. The ENTSO-E Operational Handbook [47] defines TTC as "*the maximum exchange program between two adjacent control areas that is compatible with operational security standards applied in each system if future network conditions, generation and load patterns are perfectly known in advance*". Following this definition, we propose the following model for computing the TTC from exporting zone a to importing zone b in hour

[3]Switzerland, for example, is currently sourcing primary reserve from France and Germany [42].

[4]A control area is defined as a coherent part of the interconnected system, operated by a single system operator which includes connected physical loads and/or generation units if any [1]. In the CWE system almost every bidding zone corresponds to a single control area, with the exception of the German-Austrian zone which is divided into five control areas, each one operated by a different system operator.

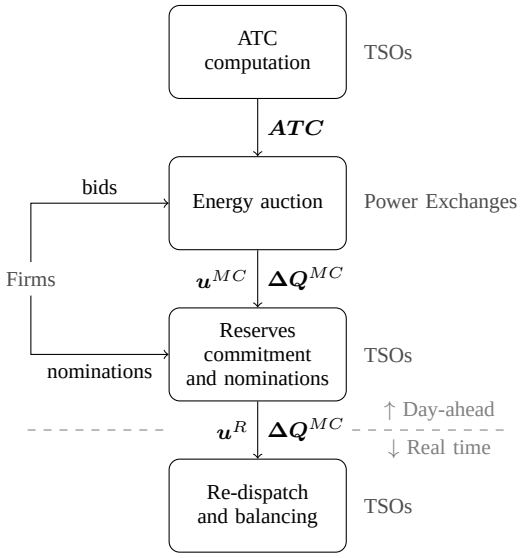

Fig. 1. Market coupling organization model overview.

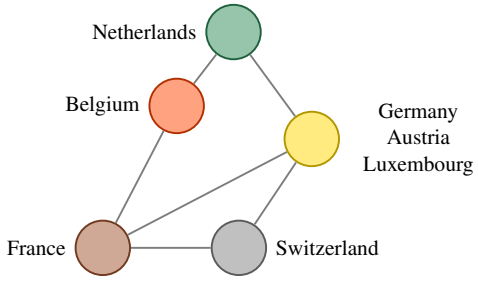

Fig. 2. Zonal model of the CWE network used by the power exchanges to clear the day-ahead energy market. Each zone is represented as a single node and exchanges between zones are limited by the ATC values.

τ, $TTC^{+}_{ab,\tau}$. The notation used in the present and subsequent mathematical formulations is described in Appendix A.

$$\max_{q,u,f,\theta} \sum_{l\in L_\times(a,b)} f_l - \sum_{l\in L_\times(b,a)} f_l \tag{1}$$

$$\text{s.t.} \sum_{l\in L_\times(c,d)} f_l - \sum_{l\in L_\times(d,c)} f_l = n^{BCE}_{(c,d),\tau} \quad \forall (c,d)\in K\setminus\{(a,b)\} \tag{2}$$

$$\sum_{g\in G(n)} q_g + \frac{1}{4}\sum_{t\in T_{15}(\tau)} \bar{\xi}_{n,t} + \sum_{l\in L(\cdot,n)} f_l = \frac{1}{4}\sum_{t\in T_{15}(\tau)} D_{n,t} + \sum_{l\in L(n,\cdot)} f_l \quad \forall n\in N \tag{3}$$

$$f_l = B_l\big(\theta_{n(l)} - \theta_{m(l)}\big)\ , \quad -F^-_l \le f_l \le F^+_l \quad \forall l\in L \tag{4}$$

$$Q^-_g u_g \le q_g \le Q^+_g u_g\ , \quad u_g\in\{0,1\} \quad \forall g\in G \tag{5}$$

$$\sum_{l\in L_\times(c,\cdot)} f_l - \sum_{l\in L_\times(\cdot,c)} f_l \le \sum_{g\in G(N(c))} Q^+_g - \big(R^{FCR}_c + R^{aFRR}_c + R^{mFRR}_c\big) - \frac{1}{4}\sum_{\substack{n\in N(c)\\ t\in T_{15}(\tau)}} \big(D_{n,t} - \bar{\xi}_{n,t}\big) \quad \forall c\in\{a,b\} \tag{6}$$

The objective function (1) corresponds to the cross-border flow (*exchange program*) from zone a to zone b, determined as the sum of individual flows over cross-border lines. Constraint (2) enforces the exchanges between other pairs of areas to correspond to a baseline value, referred to as the base case exchange (BCE). Constraint (3) enforces hourly energy balance assuming renewable supply $\bar{\boldsymbol{\xi}}$, constraint (4) models the network assuming that all lines are available, constraint (5) models generating unit output limits, considering minimum stable and maximum production.

Constraint (6) models the *operational security standards* for each control area. The left-hand-side of (6) corresponds to the net position of zone c in terms of cross-border flows, while the right-hand-side corresponds to the maximum net position for zone c such that primary, secondary and tertiary reserve targets, R^{FCR}_c, R^{aFRR}_c and R^{mFRR}_c, respectively, can be met. This constraint limits the exports of each area to a level that ensures that there is enough internal capacity to satisfy the internal demand for energy and reserves.

$TTC^{-}_{(a,b),\tau}$ (a importing, b exporting) is computed in an analogous way to $TTC^{+}_{(a,b),\tau}$, by minimizing the objective function (1). Note that in order to compute all the TTCs, problem (1)–(6) needs to be solved twice for each interconnector and hour, i.e. $2\cdot|K|\cdot|T_{60}|$ times.

Problem (1)–(6) directly maximizes the cross-border flow between a and b in a one-shot optimization problem, which outperforms iterative methods, such as the one described in [47], and methods based on net position manipulation, proposed by Neuhoff *et al.* [30].

Once the TTC value is available, the net transfer capacity $NTC^{+}_{(a,b),\tau}$ is computed by discounting the determined value for $TTC^{+}_{(a,b),\tau}$ by the Transmission Reliability Margin[5] TRM [47]. Considering a proportional TRM ($0 < TRM < 1$), common to all interconnectors, $NTC^{+}_{(a,b),\tau}$ is computed using equation (7).

$$NTC^{+}_{k,\tau} := TTC^{+}_{k,\tau} - TRM\cdot\left|TTC^{+}_{k,\tau}\right|\cdot 1_{TTC^{+}_{k,\tau}-TTC^{-}_{k,\tau}\ge TRM\cdot\left(|TTC^{+}_{k,\tau}|+|TTC^{-}_{k,\tau}|\right)} \tag{7}$$

The indicator function in equation (7) ensures that the TRM is applied only when a sufficient margin between transfer capacities in forward and backward directions exists, i.e. it guarantees that $NTC^{+}_{(a,b),\tau} \ge NTC^{-}_{(a,b),\tau}$. For computing $NTC^{-}_{(a,b),\tau}$, the TRM is added in equation (7).

NTCs are required to be simultaneously feasible, in other words, any cross-border exchange configuration respecting the NTC values must be feasible for the real network [48]. In geometric terms, the set of exchange configurations respecting the NTC values for hour τ defines a subset of $\mathbb{R}^{|K|}$, specifically an NTC hyper-rectangle $\mathcal{N}^{NTC}_{\tau} := \{\boldsymbol{n}\in\mathbb{R}^{|K|} \mid NTC^{-}_{k,\tau} \le n_k \le NTC^{+}_{k,\tau}\ \forall k\in K\}$. Simultaneous feasibility of NTCs

[5]The transmission reliability margin is defined as a security margin that copes with uncertainties on the computed TTC values arising from: (i) inadvertent deviations of physical flows during operation due to the physical functioning of secondary control; (ii) emergency exchanges between TSOs to cope with unexpected unbalanced situations in real time; (iii) inaccuracies, e.g. in data collection and measurements [1].

demands that $\mathcal{N}_\tau^{NTC}$ is fully contained within the region defined by feasible exchanges for the real network, $\mathcal{N}_\tau^{OPF}$ (a $|K|$-dimensional polyhedron). In practice, however, this requirement is relaxed and replaced by vertex feasibility[6], which demands that all vertices of $\mathcal{N}_\tau^{NTC}$ are contained within $\mathcal{N}_\tau^{OPF}$ [48].

Vertex feasibility is not necessarily satisfied by NTC values computed using equation (7), NTC values computed using other procedures proposed in the literature [30], or the procedure used in practice [47]. The technical documentation [48] states that if NTC values do not comply with vertex feasibility then "*reductions are applied to the NTC levels in a coordinated way with a view to eliminating overloads*". We model this process by computing a new set of NTC values $\boldsymbol{\chi}^+, \boldsymbol{\chi}^-$, as the solution of problem (8)–(14), which aims at achieving vertex feasibility with the minimum possible total reduction on the NTCs.

$$\min_{\chi,q,f,\theta} \sum_{k\in K} \Big(\big(NTC_{k,\tau}^{+} - \chi_k^{+}\big) + \big(\chi_k^{-} - NTC_{k,\tau}^{-}\big) \Big) \tag{8}$$

$$\text{s.t.} \quad \chi_k^{+} \le NTC_{k,\tau}^{+}\,, \quad \chi_k^{-} \ge NTC_{k,\tau}^{-}\,, \quad \chi_k^{+} \ge \chi_k^{-} \quad \forall k \in K \tag{9}$$

$$\sum_{l\in L_\times(a,b)} f_l^i - \sum_{l\in L_\times(a,b)} f_l^i = 1_{ab}^i\, \chi_{(a,b)}^{+} + (1 - 1_{ab}^i)\, \chi_{(a,b)}^{-} \quad \forall (a,b) \in K, i \in \Xi \tag{10}$$

$$\sum_{g\in G(n)} q_g^i + \frac{1}{4} \sum_{t\in T_{15}(\tau)} \bar{\xi}_{n,t} + \sum_{l\in L(\cdot,n)} f_l^i = \frac{1}{4} \sum_{t\in T_{15}(\tau)} D_{n,t} + \sum_{l\in L(n,\cdot)} f_l^i \quad \forall n \in N, i \in \Xi \tag{11}$$

$$f_l^i = B_l\big(\theta_{n(l)}^i - \theta_{m(l)}^i\big)\,, \; -F_l^{-} \le f_l^i \le F_l^{+} \;\; \forall l \in L, i \in \Xi \tag{12}$$

$$0 \le q_g^i \le Q_g^{+} \quad \forall g \in G, i \in \Xi \tag{13}$$

$$\sum_{l\in L_\times(a,\cdot)} f_l^i - \sum_{l\in L_\times(\cdot,a)} f_l^i \le \sum_{g\in G(N(a))} Q_g^{+} - \big(R_a^{FCR} + R_a^{aFRR} + R_a^{mFRR}\big) - \frac{1}{4} \sum_{\substack{n\in N(a)\\ t\in T_{15}(\tau)}} \big(D_{n,t} - \bar{\xi}_{n,t}\big) \quad \forall a \in A, i \in \Xi \tag{14}$$

The objective function (8) corresponds to the total NTC reduction, i.e. the difference between the preliminary NTC values $\boldsymbol{NTC}^{\pm}$ and the vertex feasible NTC values $\boldsymbol{\chi}^{\pm}$. The constants in this objective function drop out of the optimization and can therefore be ignored, but are included here for clarity of the exposition. Constraints (9) establish the bounds for $\boldsymbol{\chi}^{\pm}$ for all interconnectors.

Each vertex $i \in \Xi$ of $\mathcal{N}_\tau^{NTC}$ can be mapped to an array of directions for cross-border flows, e.g. [*forward* on (a,b), *backward* on (c,d), ...], hence it can be represented using an indicator 1_{ab}^i for each interconnector (a,b) with $1_{ab}^i = 1$ if flow on (a,b) goes in the forward direction in vertex i and $1_{ab}^i = 0$ otherwise. Using these indicators, constraints (10) force the cross-border flow on interconnector (a,b) at vertex $i \in \Xi$ to be equal to the corresponding vertex feasible NTC.

The requirement that all vertices $i \in \Xi$ of $\mathcal{N}_\tau^{NTC}$ are contained within $\mathcal{N}_\tau^{OPF}$ is enforced through constraints (11)–(14), which correspond to the linear relaxation of constraints (3)–(6) for each vertex. As the formulation employed is based on the vertices of $\mathcal{N}_\tau^{NTC}$, we have that in general the size of the problem is exponential in the number of interconnectors ($|\Xi| = 2^{|K|}$). For the CWE system the number of vertices to be considered is 2^6, which results in a large-scale linear problem that is still tractable using state-of-the-art linear solvers.

Since our market coupling model does not consider previously contracted transmission capacity, available transfer capacities are equal to the optimal simultaneously feasible NTCs, $ATC_{k,\tau}^{\pm} := (\chi_k^{\pm})^* \;\forall k \in K$. As a final remark, note that the solution to problem (8)–(14) might not be unique. In such a case, an auxiliary quadratic problem can be solved to obtain unique simultaneously feasible NTCs, following the methodology used in [40] to compute unique prices.

B. Day-ahead energy market clearing

Day-ahead energy market clearing in CWE is carried out by power exchanges. Exchanges collect bids from participants and determine the acceptance/rejection decisions that maximize social welfare. Energy is cleared using a strict linear pricing scheme, which results in a series of rules regarding the acceptance/rejection of different types of bids, depending on whether they are in-the-money (bid acceptance would yield a strictly positive profit), at-the-money (bid acceptance would yield zero profit) or out-of-the-money (bid acceptance would yield strictly negative profit). Currently two main types of bids are allowed by power exchanges in the CWE system:

- **Continuous bids**: bids that can be accepted partially. Continuous bids that are in-the-money must be fully accepted, at-the-money continuous bids can be partially accepted and out-of-the-money continuous bids must be rejected.
- **Block bids**: bids that can be either fully accepted or rejected (fill-or-kill condition, which gives rise to integer variables in the clearing model). Block bids that are in-the-money or at-the-money can be accepted or paradoxically rejected, while out-of-the-money block bids must be rejected.

Block bids can be arranged in linked families, in which the acceptance/rejection of certain bids is conditional on the acceptance of other bids, or in exclusive groups, in which at most one block order within the group can be accepted.

Once the bids have been collected, the power exchange clears the market using the simplified network model provided by the TSOs (Fig. 2) in order to represent cross-border exchanges.

The CWE power exchange uses the EUPHEMIA algorithm [40] to clear the energy market, based on the bids submitted by firms. In the following we present an equivalent model of EUPHEMIA proposed by Madani and Van Vyve [49], which has been modified in order to account for exclusive groups.

[6]Note that vertex feasibility corresponds to a relaxation of simultaneous feasibility if $\mathcal{N}_\tau^{OPF}$ is not convex.

Consider that buy bids (e.g. loads) correspond to bids with positive quantities $Q > 0$, while sell bids (e.g. generators) correspond to bids with negative quantities $Q < 0$. Then, the welfare maximization (market clearing) problem can be formulated as the mathematical program (15)–(21), where constraints have been grouped in primal-dual pairs.

$$\max_{\substack{x,y,n\\ s,p,\lambda}} \quad \sum_{i\in I}\Big(\sum_{\tau\in T_{60}} Q^i_\tau P^i\Big)x_i + \sum_{j\in J}\Big(\sum_{\tau\in T_{60}} Q^j_\tau P^j\Big)y_j \tag{15}$$

$$\text{s.t.} \quad \sum_{i\in I}\Big(\sum_{\tau\in T_{60}} Q^i_\tau P^i\Big)x_i + \sum_{j\in J}\Big(\sum_{\tau\in T_{60}} Q^j_\tau P^j\Big)y_j \geq \sum_{i\in I} s_i + \sum_{g\in \bar{G}} s_g + \sum_{\substack{k\in K\\ \tau\in T_{60}}}\Big(ATC^+_{k,\tau}\lambda^+_{k,\tau} - ATC^-_{k,\tau}\lambda^-_{k,\tau}\Big) \tag{16}$$

$$\sum_{i\in I(a)} Q^i_\tau x_i + \sum_{j\in J(a)} Q^j_\tau y_j = \sum_{k\in K(\cdot,a)} n_{k,\tau} - \sum_{k\in K(a,\cdot)} n_{k,\tau} \quad \forall a\in A, \tau\in T_{60} \tag{17}$$

$$ATC^-_{k,\tau} \leq n_{k,\tau} \leq ATC^+_{k,\tau}\,, \quad p_{a(k),\tau} - p_{b(k),\tau} + \lambda^+_{k,\tau} - \lambda^-_{k,\tau} = 0 \quad \forall k\in K, \tau\in T_{60} \tag{18}$$

$$x_i \leq 1\,, \quad s_i + \sum_{\tau\in T_{60}} Q^i_\tau p_{\hat{a}(i),\tau} \geq \sum_{\tau\in T_{60}} Q^i_\tau P^i \quad \forall i\in I \tag{19}$$

$$\sum_{j\in J_E(g)} y_j \leq 1 \quad \forall g\in\bar{G}\,,\; s_{g(j)} + \sum_{\tau\in T_{60}} Q^j_\tau p_{\hat{a}(j),\tau} \geq \sum_{\tau\in T_{60}} Q^j_\tau P^j - M_j(1-y_j) \quad \forall j\in J \tag{20}$$

$$\boldsymbol{x},\boldsymbol{s},\boldsymbol{\lambda}\geq 0\,;\; \boldsymbol{y}\in\{0,1\}^{|J|} \tag{21}$$

The objective function (15) corresponds to total welfare. Constraint (16) enforces strong duality at the solution, i.e. it enforces equality of the total welfare with the total surplus (surplus minimization is the dual of welfare maximization). As a consequence of Theorem 2 of [49], constraint (16) guarantees that a solution to (15)–(21) will satisfy (i) complementary slackness between the acceptance of bids and the surplus for continuous bids and accepted block bids, as well as (ii) complementary slackness between exchanges and congestion prices.

Energy balance at each area is expressed through constraints (17). Relation (18) corresponds to primal and dual constraints for exchanges in the simplified (transportation) network provided by the TSOs.

Constraints (19)–(20), together with constraint (16), establish primal restrictions and dual conditions for the acceptance of different types of bids. Constraints (19) and complementary slackness ($s_i \perp 1 - x_i$ and $x_i \perp s_i + \sum_{\tau\in T_{60}} Q^i_\tau p_{\hat{a}(i),\tau} - \sum_{\tau\in T_{60}} Q^i_\tau P^i$, $\forall i \in I$) ensure that continuous bids are accepted ($x_i = 1$) if they are in-the-money ($s_i > 0$), partially accepted ($0 \leq x_i \leq 1$) if they are at-the-money ($s_i = 0$ and $\sum_{\tau\in T_{60}} Q^i_\tau p_{\hat{a}(i),\tau} = \sum_{\tau\in T_{60}} Q^i_\tau P^i$), and rejected ($x_i = 0$) otherwise.

Constraints (20) deal with block bids within exclusive groups. Among the bids $J_E(g)$ of group g, at most one can be accepted and that bid must be in-the-money or at-the-money.

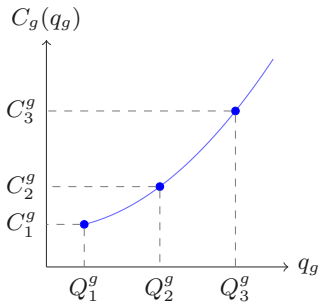

Fig. 3. Production cost function discretization. Each production level Q^g_j is associated with a production cost C^g_j through the cost function $C_g(\cdot)$.

Provided M_j are sufficiently large constants, the surplus of the group s_g is determined by the accepted bid only. The accepted bid is not necessarily the one with the maximum surplus within the group, i.e. the maximum surplus bid can be paradoxically rejected, and it is also true that the entire group can be paradoxically rejected.

C. Firm bids and energy market clearing reformulation

The solution of the market clearing model (15)–(21) complies with the rules of the CWE exchange that govern the acceptance/rejection of bids. Nevertheless, the model presumes a finite set of bids that have been bid by agents to the exchange.

In order to construct bids for all participants, we assume that they place bids in the energy market that approximate as closely as possible their feasible production/consumption possibilities[7] and their true costs/valuations. Following this assumption, loads, renewable producers and certain thermal producers can be easily modeled as submitting continuous bids.

Other thermal generators, for which we consider commitment decisions, cannot represent their constraints using continuous bids. They are modeled as submitting large exclusive groups (one group per generator) containing a discretized version of their generation possibilities for the next day. To construct this discrete set of production possibilities, the generator output is first discretized in m_g levels $\{Q^g_j\}_{j=1}^{m_g}$. The computation of production cost is accordingly discretized, as shown in Fig. 3. The first level of production corresponds to the technical minimum, the last level corresponds to the generator capacity and m_g must be large enough in order to allow the generator to ramp between different levels of output without violating its ramp rate.

The generator output at each hour τ can then be expressed as $\sum_{j=1}^{m_g} Q^g_j \omega^g_{j,\tau}$, where $\omega^g_{j,\tau}$ is an auxiliary binary variable such that $\sum_{j=1}^{m_g} \omega^g_{j,\tau} \leq 1$, $\forall\tau\in T_{60}$ [50]. Any production profile within the discrete set is then defined by a certain $\boldsymbol{\omega}^g$. In order to be a feasible production profile, the production, commitment and startup associated with a certain production profile must comply with the generator constraints: technical minimum, maximum capacity, minimum up/down times and ramp rate

[7]Bidding infeasible production/consumption bids would conflict with the rules of the power exchange [39].

constraints. These constraints define the hourly production domain $\mathcal{D}_g^{60}$.

Considering that each feasible production profile of generator g is included in group g, we can reformulate the energy clearing model as problem (22)–(27), where $h_g(\boldsymbol{\omega}_g, \boldsymbol{v}_g)$ corresponds to the total cost of the production profile associated with $\boldsymbol{\omega}_g$ and $\boldsymbol{v}_g$, and where $\boldsymbol{v}_g$ corresponds to the startup indicator variable. Problem (22)–(27) explicitly includes hourly approximations of the unit commitment constraints for thermal generators while respecting the rules of the power exchange for the treatment of non-convexities.

$$\max_{\substack{x,\omega,v,n\\ s,p,\lambda}} \quad \sum_{i\in I}\left(\sum_{\tau\in T_{60}} Q_\tau^i P^i\right)x_i - \sum_{g\in\bar{G}} h_g(\boldsymbol{\omega}_g,\boldsymbol{v}_g) \tag{22}$$

$$\text{s.t.} \quad \sum_{i\in I}\left(\sum_{\tau\in T_{60}} Q_\tau^i P^i\right)x_i - \sum_{g\in\bar{G}} h_g(\boldsymbol{\omega}_g,\boldsymbol{v}_g) \geq \sum_{i\in I} s_i + \sum_{g\in\bar{G}} s_g + \sum_{\substack{k\in K\\ \tau\in T_{60}}}\left(ATC_{k,\tau}^{+}\lambda_{k,\tau}^{+} - ATC_{k,\tau}^{-}\lambda_{k,\tau}^{-}\right) \tag{23}$$

$$\sum_{i\in I(a)} Q_\tau^i x_i - \sum_{g\in G(N(a))}\sum_{j=1}^{m_g} Q_j^g \omega_{j,\tau}^g = \sum_{k\in K(\cdot,a)} n_{k,\tau} - \sum_{k\in K(a,\cdot)} n_{k,\tau} \quad \forall a\in A, \tau\in T_{60} \tag{24}$$

$$\sum_{j=1}^{m_g}\omega_{j,\tau}^g \leq 1 \quad \forall g\in\bar{G}, \tau\in T_{60}\,,$$

$$s_g \geq \sum_{\tau\in T_{60}}\sum_{j=1}^{m_g} Q_j^g\omega_{j,\tau}^g p_{\hat{a}(g),\tau} - h_g(\boldsymbol{\omega}_g,\boldsymbol{v}_g) \quad \forall g\in\bar{G} \tag{25}$$

$$\left(\sum_{j=1}^{m_g} Q_j^g\boldsymbol{\omega}_j^g\,,\ \sum_{j=1}^{m_g}\boldsymbol{\omega}_j^g\,,\ \boldsymbol{v}_g\right) \in \mathcal{D}_g^{60} \quad \forall g\in\bar{G} \tag{26}$$

$$(18)\text{–}(19);\ \boldsymbol{x},\boldsymbol{s},\boldsymbol{\lambda}\geq 0\,;\ \boldsymbol{\omega}^g\in\{0,1\}^{m_g\times|T_{60}|}\ \forall g\in\bar{G} \tag{27}$$

Problem (22)–(27) is analogous to (15)–(21), with the difference that block bids that were explicitly enumerated in (20) are now implicitly enumerated by (25)–(26). Constraint (25) ensures that each generator recovers at least its production cost, while constraint (26) enforces that the accepted production profile is feasible. We define the total cost function $h_g(\boldsymbol{\omega}_g, \boldsymbol{v}_g)$ according to equation (28).

$$h_g(\boldsymbol{\omega}_g,\boldsymbol{v}_g) := \sum_{\tau\in T_{60}}\left(\sum_{j=1}^{m_g} C_j^g\omega_{j,\tau}^g + K_g\sum_{j=1}^{m_g}\omega_{j,\tau}^g + S_g v_{g,\tau}\right) \tag{28}$$

Notice that constraint (25) includes a product of two variables, $\omega_{j,\tau}^g p_{\hat{a}(j),\tau}$, which can be linearized by using a big-M formulation since $\omega_{j,\tau}^g$ is binary [50].

The solution of the energy clearing model of equations (22)–(27) determines the preliminary commitment $\boldsymbol{u}_g^{MC}$ for slow generators and net positions $\boldsymbol{\Delta Q}_a^{MC}$ for each zone. The net position can be computed using equations (29) and (30).

$$u_{g,\tau}^{MC} := \sum_{j=1}^{m_g}(\omega_{j,\tau}^g)^* \quad \forall g\in G_{SLOW}, \tau\in T_{60} \tag{29}$$

$$\Delta Q_{a,\tau}^{MC} := \sum_{\substack{g\in\\ G(N(a))}}\sum_{j=1}^{m_g} Q_j^g(\omega_{j,\tau}^g)^* - \sum_{i\in I(a)} Q_\tau^i x_i^* \ \forall a\in A, \tau\in T_{60} \tag{30}$$

We conclude this subsection by pointing out that the solution of (22)–(27) represents an optimistic situation in which the power exchange can decide among a large number of possible schedules in order to maximize welfare. Limits on the number of profiles that each unit can bid into the market can also be included in the formulation or during the solution of the energy clearing problem.

D. Reserves

Reserves in the CWE region can be classified into three categories: (i) primary reserves (also referred as Frequency Containment Reserve or FCR) are responsive to frequency and must be delivered within 30 seconds; (ii) secondary reserves (also referred to as automatic Frequency Restoration Reserves or aFRR) are activated following the activation of FCR, and must be delivered within 5-15 minutes; and (iii) tertiary reserves (also referred to as manual Frequency Restoration Reserves or mFRR) must be delivered within 15-30 minutes.

Following the assumption of harmonization in the definition of reserve products across zones [6], we model the reserve allocation and nomination process [44], [45] as a simultaneous cost minimizing scheduling that aims at securing the requisite FCR, aFRR and mFRR capacity. This scheduling is conducted at day ahead in each zone, after the clearing of the energy market, where firms can also trade their production obligations. This is in line with current operating practice in Belgium, France, Germany and Switzerland. Given that balancing responsible parties are required to offer reserve while maintaining a balanced position [17], [41], we assume that the reserve scheduling must honor the net positions determined by the power exchange $\Delta Q_{a,\tau}^{MC}$ for each zone and period. Additionally, we assume that slow generators committed by the power exchange cannot be shut down when reserves are allocated.

Considering these assumptions, the commitment of reserve capacity for each 15-minute interval of the following day is formulated as the optimization problem (31)–(35), which needs to be solved separately for each zone in the system.

$$\min_{q,r,u,v}\ \sum_{g\in G(N(a))}\left(\frac{1}{4}\sum_{t\in T_{15}} C(q_{g,t}) + \sum_{\tau\in T_{60}}\left(K_g u_{g,\tau} + S_g v_{g,\tau}\right)\right) \tag{31}$$

$$\text{s.t.} \quad \sum_{g\in G(a)} r_{g,t}^{FCR} \geq R_a^{FCR}\,,$$

$$\sum_{g\in G(a)}\left(r_{g,t}^{FCR} + r_{g,t}^{aFRR}\right) \geq R_a^{FCR} + R_a^{aFRR}\,,$$

$$\sum_{g\in G(a)}\left(r_{g,t}^{FCR} + r_{g,t}^{aFRR} + r_{g,t}^{mFRR}\right) \geq R_a^{FCR} + R_a^{aFRR} + R_a^{mFRR} \quad \forall t\in T_{15} \tag{32}$$

$$\sum_{\substack{g\in G(N(a))\\ t\in T_{15}(\tau)}} q_{g,t} + \sum_{\substack{n\in N(a)\\ t\in T_{15}(\tau)}} \left(\bar{\xi}_{n,t} - D_{n,t}\right) = 4\Delta Q^{MC}_{a,\tau} \;\; \forall \tau \in T_{60} \tag{33}$$

$$u_{g,\tau} \geq u^{MC}_{g,\tau} \quad \forall g \in G_{\text{SLOW}}(N(a)), \tau \in T_{60} \tag{34}$$

$$\left(\boldsymbol{q}_g, \boldsymbol{r}^{FCR}_g, \boldsymbol{r}^{aFRR}_g, \boldsymbol{r}^{mFRR}_g, \boldsymbol{u}_g, \boldsymbol{v}_g\right) \in \mathcal{D}^{15,R}_g \;\; \forall g \in G(N(a)) \tag{35}$$

The objective function (31) corresponds to the total cost of the planned operation of zone a. Constraint (32) enforces the reserve requirements for each period. Constraint (33) requires that each zone maintains its day-ahead position in the energy market, and constraint (34) requires that slow units committed by the energy exchange remain ON during the commitment of reserves. Constraint (35) corresponds to generator constraints for providing energy and reserves that must be respected with a 15-minute time resolution.

The reserve allocation (31)–(35) can modify the output of the energy market clearing model by turning on additional slow generators to supply reserves. Consequently, the output of the reserve allocation is a new vector of commitment for slow generators $\boldsymbol{u}^R, \boldsymbol{v}^R$, which guarantees the availability of the required reserves for each zone and for each period of the next day.

E. Redispatch and balancing

During real-time operations, Kirchhoff's laws determine the flows on the network. Moreover, renewable energy supply can differ from its forecast $\bar{\boldsymbol{\xi}}$. To mitigate the effects of network congestion and forecast errors, the system operator can modify dispatch decisions and the commitment of fast generators with the objective of minimizing the real-time operating cost.

In order to evaluate the real-time cost performance of the day-ahead commitment decisions, the actual renewable injection is assumed to be modeled by the random vector $\boldsymbol{\zeta}$. The real-time operating cost of the system is then estimated by solving the redispatch and balancing model (36)–(42). The average performance of the system is estimated through Monte Carlo simulation, i.e. problem (36)–(42) is solved for each $\boldsymbol{\zeta}_s,\ s \in S_{\text{sim}}$, where S_{sim} is the set of random samples.

$$\min_{\substack{q,u,v,\delta\\ f,\theta,e,o}} \sum_{g\in G}\left(\frac{1}{4}\sum_{t\in T_{15}} C_g(q_{g,t}) + \sum_{\tau\in T_{60}}\left(K_g u_{g,\tau} + S_g v_{g,\tau}\right)\right) + V\sum_{n\in N}\sum_{t\in T_{15}} e_{n,t} + CL\sum_{a\in A}\sum_{\tau\in T_{60}}\delta_{a,\tau} \tag{36}$$

$$\text{s.t.} \quad \delta_{a,\tau} \geq \left| 4\Delta Q^{MC}_{a,\tau} - \left(\sum_{\substack{l\in L_\times(a,\cdot)\\ t\in T_{15}(\tau)}} f_{l,t} - \sum_{\substack{l\in L_\times(\cdot,a)\\ t\in T_{15}(\tau)}} f_{l,t}\right)\right| \;\; \forall a \in A, \tau \in T_{60} \tag{37}$$

$$\sum_{g\in G(n)} q_{g,t} + \zeta_{n,s,t} + \sum_{l\in L(\cdot,n)} f_{l,t} + e_{n,t} = D_{n,t} + \sum_{l\in L(n,\cdot)} f_{l,t} + o_{n,t} \quad \forall n \in N, t \in T_{15} \tag{38}$$

$$f_{l,t} = B_l\left(\theta_{n(l),t} - \theta_{m(l),t}\right), \quad -F^-_l \leq f_{l,t} \leq F^+_l \quad \forall l \in L, t \in T_{15} \tag{39}$$

$$0 \leq o_{n,t} \leq \sum_{g\in G(n)} q_{g,t} + \zeta_{n,s,t}\,, \quad 0 \leq e_{n,t} \leq D_{n,t} \quad \forall n \in N, t \in T_{15} \tag{40}$$

$$(\boldsymbol{q}_g, \boldsymbol{u}_g, \boldsymbol{v}_g) \in \mathcal{D}^{15}_g \quad \forall g \in G \tag{41}$$

$$\boldsymbol{u}_g = \boldsymbol{u}^R_g,\ \boldsymbol{v}_g = \boldsymbol{v}^R_g \quad \forall g \in G_{\text{SLOW}} \tag{42}$$

Problem (36)–(42) commits fast units, with the additional requirement of respecting day-ahead zonal net positions and the commitment schedule of slow generators. The requirement of respecting the zonal day-ahead net positions is imposed as a soft constraint, the violation of which is penalized through an L1 penalty term defined by equation (37). Assuming that, in practice, TSOs prefer to redispatch any generator instead of violating their net position, the penalty CL can be established as the maximum marginal cost of any generator within a zone. In contrast, the requirement of respecting the day-ahead commitment of slow generators is imposed as a hard constraint in equation (42).

By maintaining day-ahead zonal net positions, the redispatch and balancing model (36)–(42) captures the partial coordination of system operators in real time.

III. Numerical simulation settings

A. The Central Western European system

A number of studies have focused on developing representative models for the European grid. Leuthold [51] and Hutcheon and Bialek [52] model the European transmission grid based on study models and maps published by ENTSO-E [1] and by national TSOs, while Egerer *et al.* [53] document the existing available information on transmission, generation and demand in Europe.

We use the transmission network model of Hutcheon and Bialek [52] for the CWE system, presented in Fig. 4. Thermal ratings for cross-border lines were updated to their current values, as published in [54]. Thermal ratings for internal lines within the Netherlands were established as published in [55]. Thermal ratings for internal lines within other countries were estimated through an iterative process of simulating system operations and correcting internal capacities, with the objective of approximating the congestion management costs for the year 2015 [1].

The network was populated using an industrial database of thermal generators, provided by ENGIE, which includes technical and economic characteristics of 656 generating units. Thermal generators were assigned to network buses according to their approximate geographical location [56]. These units are classified into *five* groups: 87 nuclear units (85G W), 144 combined heat and power (CHP) units (40 GW), 272 slow

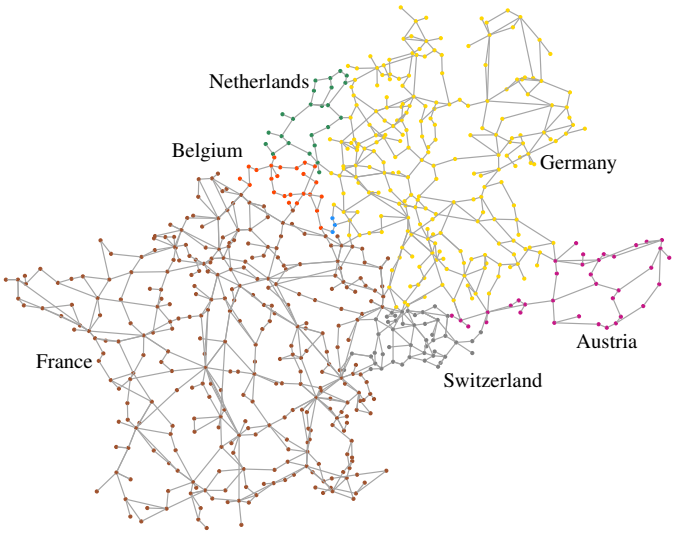

Fig. 4. Nodal model of the CWE network [52]. The model comprises the high voltage networks of the 7 countries in the CWE system, it includes 679 nodes and 1073 lines.

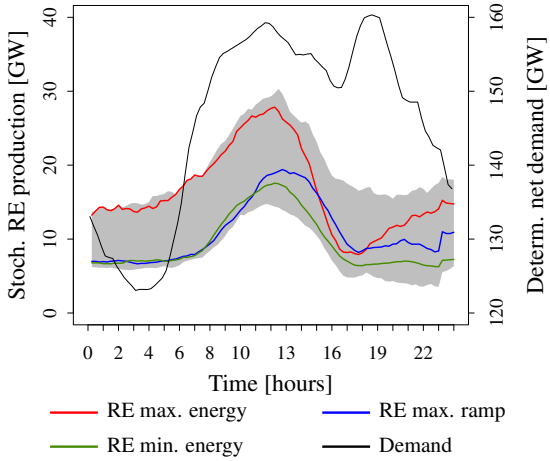

Fig. 5. Stochastic renewable energy production (wind and solar) and deterministic net demand (demand minus hydro power) for a typical autumn weekday. The shaded gray area, included in the background, shows the variation range of renewable energy production.

units (conventional thermal units that are neither nuclear nor CHP, and obey a minimum up and down time greater than 3 hours, totaling 99 GW), 126 fast units (conventional thermal units that are neither nuclear nor CHP, and obey a minimum up and down time less than or equal to 3 hours, totaling 14 GW) and 27 aggregated small generators (10 GW).

The capacity of thermal generators within Germany, France and Belgium was reduced in order to account for scheduled maintenance and large outages. A different outage de-rating factor was computed for each generator and each season based on the outage information published by national TSOs [57], [58] and Power Exchanges (PX) [59] for the year 2014.

Zonal reserve targets were obtained from [6] for Belgium, Germany and the Netherlands, and from national TSOs for other countries [42], [57], [60]. We assume that FCR needs to be delivered within 30 seconds of activation (current specification in all CWE countries), that aFRR needs to be delivered within 5 minutes of activation (current product specification in Germany), and that mFRR needs to be delivered within 15 minutes of activation (current product specification in Belgium, Germany, the Netherlands and Switzerland).

Historical 15-minute demand profiles for 2014 were collected from national TSOs for Austria [60], France [57], Belgium [58] and the Netherlands [61], and hourly demand profiles for Germany and Switzerland were collected from ENTSO-E [1]. Demand profiles were distributed across the buses of the network within the relevant area using the participation factors included in [52]. Exchanges between CWE countries and non-CWE countries are collected from [1] and are modeled as fixed flows of power at the corresponding borders.

Regional 15-minute production profiles and day-ahead forecasts for wind and solar PV for years 2013-2014 were also collected from national TSOs and power exchanges. The spatial resolution of renewable production data varies from country to country. There are 4 geographical regions in Germany, 21 regions in France, 2 regions in Belgium and 1 region in Austria. Profiles for the Netherlands and Switzerland were estimated by averaging data of neighboring regions. Offshore wind power profiles were associated to offshore wind connection buses in the transmission system. Onshore wind and solar PV capacity was distributed uniformly among generation and load buses within each administrative region of each country (12 states of Germany, 21 regions of France, 2 regions of Belgium, Austria, Switzerland and the Netherlands). Each bus with renewable capacity was then assigned a wind and a solar PV production profile according to its location, therefore the spatial information of renewable resource dispersion is preserved in our data set.

Hydro power resources are modeled as fixed injections or withdrawals from the transmission system. Hydro production profiles for seasonal storage, pumped storage and run of river were collected from RTE [57] for each power plant in France. Hydro plants in other countries were assigned production profiles based on profiles of French hydro plants and by taking into account the characteristics of these plants (technology, size and location).

We used clustering to select 8 representative day types of load for 2014, corresponding to one weekday and one weekend day for each season. We used the forecast errors of 2013-2014 to generate samples of real-time renewable energy production. Fig. 5 presents the resulting deterministic net demand and uncertainty faced by the system in the day ahead. The net load forecast error can span more than 15 GW and can exhibit ramps of up to 3 GW in 15 minutes. Renewable production ramps of this magnitude already occur in Germany, for instance in May 11, 2014, between 17:45 and 18:00 [59].

B. Simulation setup

We simulate system operation of the CWE system under three major policy designs: (*i*) the market coupling policy, which is the current zonal design in the CWE system, (*ii*) deterministic unit commitment, which is the current nodal

design in several US markets, and (*iii*) stochastic unit commitment, which is an ideal benchmark. Operations under these three designs are modeled in two stages. The first stage takes place in the day ahead and determines the commitment of the slow thermal generators based on a forecast for renewable energy supply. The second stage takes place in real time and corresponds to the re-dispatch and balancing performed by the system operator given the realization of multi-area renewable supply. The second stage must respect the commitment determined for slow thermal generators in the first stage in all policies.

Thermal generators, other than slow generators, are modeled as follows. The commitment of nuclear generators is decided prior to the day ahead, therefore it is considered as being fixed in the simulations. Similarly, CHP production is determined based on heat demand and CHP units can adjust their production only within a limited range, therefore we fix their output and allow an adjustment of $\pm 5\%$ of their capacity in the simulations. fast units adjust both their commitment and production in real time. Aggregated generators correspond to small producers, therefore no commitment decision is associated with them and it is assumed that they can adjust their production in real time.

The market coupling policy is simulated using the model described in section II. Note that while day-ahead markets are cleared using the zonal network of Fig. 2, real-time operation is simulated using the nodal network of Fig. 4. We consider two variants of the market coupling design, representing different levels of coordination in real-time redispatch and balancing: (*i*) *MC Net Position* penalizes deviations from day-ahead zonal net positions at the maximum marginal cost of any generator in the system [8], representing the operational practice whereby balancing responsible parties are required to balance their resources in real time, which implies that each zone should maintain its trading position on the day-ahead market. (*ii*) *MC Free* allows for adjustments in zonal net positions at no penalty ($CL = 0$). This approximates the effect of intra-day markets that allow balancing responsible parties to adjust their positions as real time approaches and the conditions of the system are gradually revealed, as well as the effect of coordinating balancing among zones.

Deterministic and stochastic unit commitment are modeled following [34]. Deterministic unit commitment corresponds to a centralized nodal market design with full coordination of the various products of the market (energy, reserves and transmission) and full coordination among zones. The stochastic unit commitment model additionally endogenizes the uncertainty faced by the system in order to optimally adapt the commitment of reserves to multi-area renewable supply uncertainty. We selected 25 scenarios for the stochastic unit commitment model from the real-time renewable energy production samples, by resorting to the scenario selection algorithm of Heitsch and Römisch [62]. For these two models we used a hybrid time resolution with hourly commitment decisions and quarterly dispatch decisions.

In order to estimate the performance of each policy, we perform a Monte Carlo simulation over a set of 120 samples of multi-area renewable production. We resort to high performance computing in order to parallelize the Monte Carlo simulations. The relative performance of stochastic unit commitment, deterministic unit commitment and *MC Free* is due to the difference in their day-ahead commitment schedules. The performance of *MC Net Position* is additionally affected by the requirement of adhering, in real time, to day-ahead financial positions.

Mathematical programs are implemented in Mosel/XPress [63] and solved on the Sierra cluster at the Lawrence Livermore National Laboratory. Given that we model production cost as a piece-wise linear convex function, all mathematical programs correspond either to LPs or MILPs. Most mathematical programs are solved directly by XPress, with two exceptions. (*i*) Stochastic unit commitment is solved within a 1% optimality gap using the distributed asynchronous algorithm proposed in [64] on 4 nodes. Solution times range from 44 minutes to 1 hour and 56 minutes. Each scenario subproblem consists of 444 thousand continuous variables, 539 thousand constraints and 9.5 thousand integer variables. (*ii*) The market clearing model is solved using an enumeration heuristic based on column-and-constraint generation. The heuristic achieves a cost which is within 1% of the optimal cost, and optimal welfare which is within $10^{-4}\%$ of optimal.

IV. Model validation

In order to validate the accuracy of the market coupling model, we compare the results of *MC Net Position* against the historical performance of the CWE system, as reported in publicly accessible statistics. Table I presents the actual production mix of 2014 [57], [58], [65], [66] and the resulting production mix of our model, which is obtained by averaging all samples, seasons and day types (where the contribution of each day type is weighted by the relative frequency of occurrence of each day type).

These results present a reasonable approximation to the actual production mix. The most notable differences appear in the coal production of Germany, the nuclear production of France and the conventional thermal production of the Netherlands. These differences can arise from a number of factors: (*i*) we simulate 960 days of operations over 8 representative day types in our simulation in order to exploit high performance computing and keep the study computationally tractable; (*ii*) the observed estimates of 2014 are subject to statistical error (since they correspond to 365 daily samples of operation, rather than a long-run average); (*iii*) we derate units by season instead of modeling unit-by-unit maintenance and outages, in order to capture their average effect in a season while using representative day types; (*iv*) we compute ATC values endogenously within our model, instead of using the ATCs that were used in the exchange. Notable differences between our model and the ATC values have been observed in the border between Germany and the Netherlands. In order to test the influence of ATC value differences, we have also simulated the operation of the *MC Net Position* model using the actual ATCs [1]. The results better approximate the production mix for the Netherlands and France, however the approximation of the German fuel mix worsens and the average operating cost

TABLE I
ANNUAL ENERGY PRODUCTION BY PRIMARY SOURCE

Country	Primary source	MC Net Pos. results [TWh]	System statistics [TWh]
Germany	Coal	234.2	274.1
	Nuclear	87.0	97.1
	Gas	11.2	59.8
	Wind	44.4	57.3
	Solar	39.4	35.1
	Hydro	13.1	19.6
	Oil	0.2	6.1
	Other	64.3	75.9
France	Nuclear	468.0	415.5
	Hydro	55.0	67.3
	Wind	16.0	17.1
	Gas	3.0	13.1
	Coal	11.6	6.7
	Solar	5.9	5.8
	Oil	0.0	2.6
	Other	27.2	7.4
Netherlands	Thermal	38.0	91.1
	Wind	6.2	5.8
	Nuclear	4.1	4.1
	Hydro	0.1	0.1
	Solar	0.8	–
Switzerland	Hydro	32.4	37.5
	Nuclear	22.3	25.4
	Thermal	5.2	3.7
	Wind & Solar	0.9	–
Belgium	Nuclear	26.7	32.1
	Thermal	13.2	23.9
	Solar	3.4	2.8
	Wind	4.7	2.5
	Hydro	0.3	1.4
Austria	Hydro	34.5	40.2
	Thermal	13.2	13.8
	Wind	4.0	3.0
	Solar	0.5	–
Total		1291.2	1447.8

increases by 8.4%, due to a significant shift in production from France-Germany (where energy is produced at a low marginal cost) to Belgium-Netherlands (where energy is produced at a higher marginal cost). We therefore use the ATC values computed endogenously by our model, in order to maintain ATC values that are internally consistent with the CWE transmission model that we use in our simulations.

In addition to fuel mix, we compare the congestion management costs estimated by our model to those published by national TSOs. We estimate the congestion management costs as the difference between the cost of *MC Net Position* with and without thermal limits on lines. Table II presents a comparison between the estimated congestion management costs and the actual congestion management costs of the CWE system[8] [1] (values correspond to January-December 2015). The congestion management costs estimated by our model correctly approximate the current situation of the Germany-Austria bidding zone, although they are greater than those observed in reality for Belgium and France. We note that our model does not account for the active control of transmission networks for relieving congestion (e.g. the use of FACTS devices at the borders and transmission switching in Belgium [67]). The integration of active transmission network management in our model is an area of future research.

[8]Congestion management costs that cover most of the CWE area were not available for 2014.

TABLE II
CONGESTION MANAGEMENT COSTS

Zone	MC Net Pos. results [MM€/year]	System statistics [MM€/year]
DE/AT/LX	679.2	688.2
Belgium	118.4	0.0
France	66.4	1.1
Netherlands	19.4	–
Switzerland	8.7	–

TABLE III
EXPECTED POLICY COSTS AND EFFICIENCY LOSSES WITH RESPECT TO DETERMINISTIC UC

Policy	Expected cost [MM€/d]	Efficiency losses [%]	[MM€/year]
MC Net Position	30.42	6.2	650
MC Free	29.45	2.8	294
Deterministic UC	28.64	–	–
Stochastic UC	28.49	–0.5	–55
Perfect Foresight	28.32	–1.1	–117

V. POLICY ANALYSIS RESULTS

We proceed with a comparison of the cost performance of the four policies described in section III-B: stochastic unit commitment, deterministic unit commitment, *MC Free* and *MC Net Position*.

The average cost of each policy is presented in Table III. In addition, the cost of perfect foresight is provided for comparison. The difference between *MC Net Position* and *MC Free* quantifies the benefits of intra-day markets and the coordination of TSOs in balancing. These efficiency gains are estimated at 3.4% of operating costs. The difference between *MC Free* and deterministic unit commitment quantifies the efficiency gains of nodal market design relative to zonal markets, and is estimated at 2.8% of operating cost. Finally, the difference between deterministic and stochastic unit commitment corresponds to the benefits of endogenizing uncertainty relative to using fixed requirements for the commitment of reserves. This gain amounts to 0.5%. Even when considering the perfect foresight model, gains of perfectly forecasting uncertainty are no larger than 1.1%. These gains are notably lower than the aforementioned cost differences between deterministic unit commitment, *MC Free* and *MC Net Position.*

The breakdown of operating costs is presented in Table IV, where SLOW$^+$ corresponds to the set of nuclear, CHP, slow and aggregated units. We note that the differences between policies are largely driven by the production cost of fast units, with the market coupling policies incurring substantially higher costs from fast units relative to deterministic unit commitment. Differences between deterministic and stochastic unit commitment are driven largely by differences in the commitment cost of slow units.

Table V presents the expected production of each generator type along with the production-weighted average marginal cost of units providing energy. We note that even though production from fast units is limited to 0.7–1.4% of the total production,

TABLE IV
COMPOSITION OF THE EXPECTED OPERATING COST

Policy	Commitment cost [MM€/d]		Production cost [MM€/d]		Load shedding [MM€/d]
	SLOW+	FAST	SLOW+	FAST	
MC Net Pos.	2.83	0.28	25.60	1.61	0.10
MC Free	2.83	0.20	25.39	0.97	0.05
Determ. UC	2.81	0.07	25.45	0.31	0.00
Stoch. UC	2.60	0.12	25.21	0.56	0.00

TABLE V
PRODUCTION AND AVERAGE MARGINAL COST OF THERMAL GENERATORS PER POLICY

Policy	Production [TWh/year]		Production curtailment [TWh/year]	Av. marginal cost [€/MWh]	
	SLOW+	FAST		SLOW+	FAST
MC Net Pos.	1014.9	14.6	6.5	9.21	40.14
MC Free	1014.1	11.3	2.4	9.14	31.34
Determ. UC	1016.8	7.4	1.2	9.14	15.29
Stoch. UC	1015.4	9.0	1.3	9.06	22.99

the production cost of fast units corresponds to 1.2–6.3% of the total production cost. This table highlights the fact that the market coupling policies often resort to the activation of a substantial amount of fast units that are found at the far right of the fast unit supply stack. This large increase in the production costs of fast units is accompanied by an increasing amount of production curtailment that is required for alleviating congestion and balancing zones in *MC Net Position*.

We proceed with analyzing a number of factors that could explain the substantial observed cost differences among deterministic unit commitment, *MC Free* and *MC Net Position*[9]. In order to better understand the results, we compare the models in pairs, moving from the most efficient to the least efficient policy.

A. Relative performance of deterministic unit commitment and MC Free

The MC design and deterministic unit commitment schedule similar amounts of slow capacity within each area, in all day types. The amount of committed capacity is mostly driven by the net demand of each area. Nevertheless, the units committed by *MC Free* are less useful in real time, as can be seen in Fig. 6. Units that are committed by *MC Free* and not by deterministic unit commitment remain at their technical minimum for more than 85% of the time, and are used at full capacity for less than 5% of the time. Units committed by deterministic unit commitment and not by *MC Free*, in contrast, are used significantly more.

The commitment decisions of *MC Free* are mainly driven by the merit order of different units within each area, while ignoring intra-zonal flows and misrepresenting the physical laws governing cross-border exchanges. This leads to schedules that are not necessarily feasible when considering the full network, as shown in Fig. 7. Slow units that are committed by *MC Free* and result in congestion need to be re-dispatched down in real

[9]Differences between the stochastic and deterministic UC have been analyzed in the literature [34].

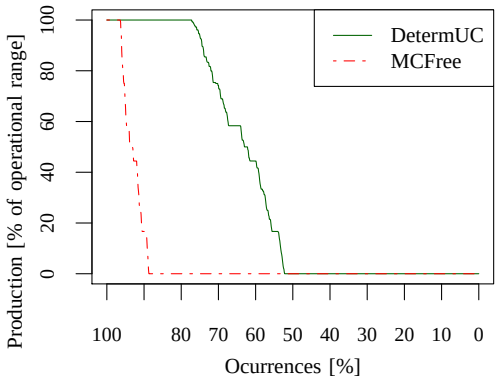

Fig. 6. Production duration curves of slow units that are exclusively committed by deterministic unit commitment and *MC Free*. For any online unit, 0% of the operational range corresponds to its technical minimum while 100% corresponds to its maximum capacity. In green, slow units that were committed by deterministic unit commitment but not by *MC Free*. In red (dashed), slow units committed by the market coupling model but not by deterministic unit commitment.

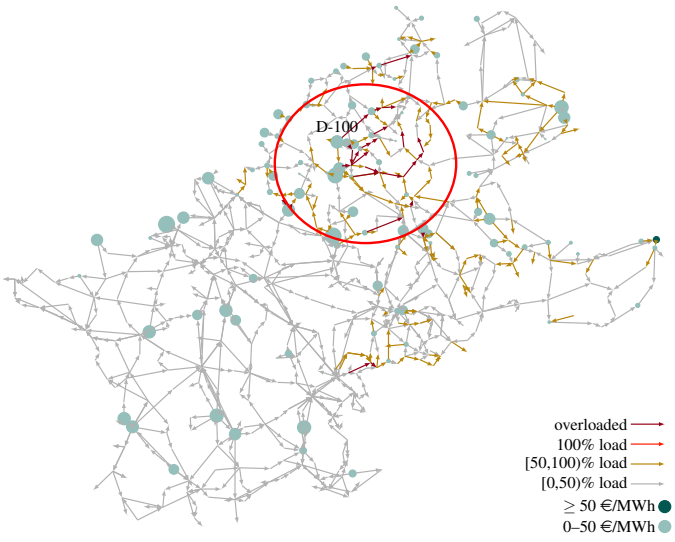

Fig. 7. Day-ahead schedule determined by *MC Free* for a spring weekday at the 17:00–18:00 interval. Flows implied by the production schedule are infeasible for the real network since they overload lines in the west of Germany. This infeasible schedule is altered in real time by re-dispatching all generators at D-100 down to their technical minimum and starting up fast units in the surrounding area in order to relieve congestion.

time in order to prevent overloading transmission lines. This results in the activation of more expensive units in real time relative to deterministic unit commitment.

Fig. 8 demonstrates that congestion management after day-ahead market clearing results in a more frequent use of high-cost fast units in the case of *MC Free*. Deterministic unit commitment, on the other hand, does not require a substantial modification of the day-ahead schedule in real time since the physical constraints of the transmission network are accounted for when committing slow generators (the same is true for stochastic unit commitment), as it is the case in nodal US markets [11]. This highlights the need to account for unit commitment when analyzing zonal market designs, a feature

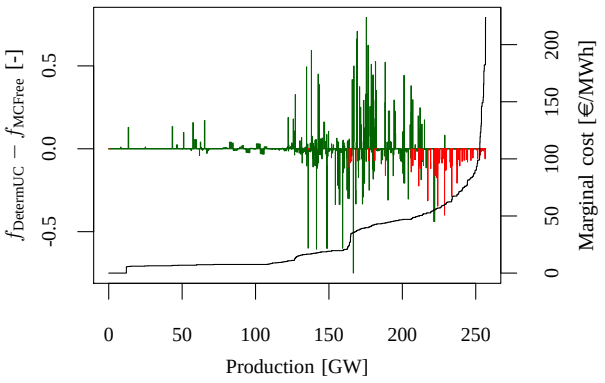

Fig. 8. Difference in the frequency of use of supply curve increments between deterministic unit commitment and the *MC Free* policy for autumn weekdays. The frequency of use of each supply increment, for a given policy and day type, corresponds to the proportion of the increment that is used on average over all quarterly periods and all samples of real-time operation. In the plot, green stripes represent the frequency of use of supply increments corresponding to SLOW$^+$ generators, while red stripes correspond to fast generators. The marginal cost function of the system (which is measured in the right vertical axis) is presented for reference in black.

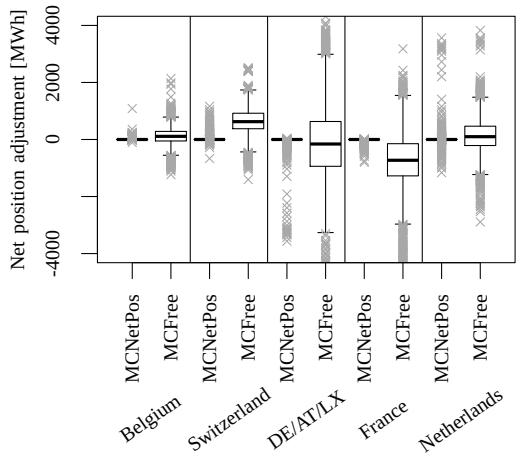

Fig. 9. Adjustment of zonal net position in real time with respect to the day-ahead net position. A positive adjustment corresponds to a real-time net position that is larger than the day-ahead net position, and vice versa. Net position adjustments of DE/AT/LX range between -6 GW and 5 GW.

that has been largely overlooked in existing literature.

B. Relative performance of MC Free and MC Net Position

The comparison of *MC Net Position* and *MC Free* provides an indication about the value of intra-day adjustments and the coordination of TSOs in balancing operations [6]. Fig. 9 demonstrates that *MC Free* continuously alters the day-ahead net position due to the coordination among zones, whereas *MC Net Position* only deviates from the day-ahead zonal net positions in extreme situations (these correspond to outliers in the box plots).

The behavior of the *MC Net Position* model is largely driven by the renewable supply forecast error of DE/AT/LX (more specifically Germany), since adjustment in other zones is driven by adjustments in DE/AT/LX. This is demonstrated

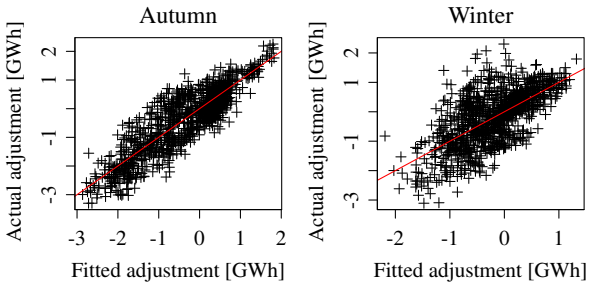

Fig. 10. Linear regression of the adjustment of the real-time net position of DE/AT/LX under *MC Free* relative to *MC Net Position* for autumn weekdays (best fit) and winter weekdays (worst fit). The explanatory variables are the forecast error of DE/AT/LX and the day-ahead net positions of the zones. A 45 degree line is drawn in red along with the data for comparison.

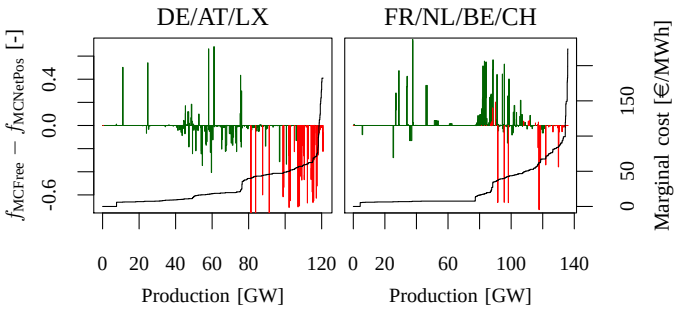

Fig. 11. Difference in use of zonal supply function increments between *MC Free* and *MC Net Position*, for samples and periods with an adjustment of the net position of DE/AT/LX below the 87.5% quantile (12.5% larger reductions in net position of DE/AT/LX), for autumn weekdays.

in Fig. 10. The figure presents the linear regression of the adjustments in the DE/AT/LX zone, using the forecast error in renewable production and the day-ahead net positions as independent variables. Across all day types, the forecast error (with positive correlation) and the day-ahead net position of DE/AT/LX (with negative correlation) are the factors with the greatest coefficients and highest significance levels. This indicates that when DE/AT/LX is short on its prediction of renewable supply (negative forecast error) and has available import capacity (large day-ahead net position), the *MC Free* policy will decrease the real-time net position of the zone by importing more power from other areas. Instead, according to the *MC Net Position* policy the forecast error is corrected by re-dispatching within the zone, which results in significantly higher cost, as can be observed in Fig. 11. This highlights a major weakness of partial real-time coordination in systems with substantial levels of renewable supply, which can result in major efficiency losses. Note that this type of efficiency loss affects both the continental European system as well as the wide interconnections in US systems [16].

VI. Conclusions

In this paper we propose a hierarchy of mathematical programs that model the sequential clearing of products in zonal electricity markets, in particular, the market coupling design currently present in continental Europe. Our model accounts

for the simplified representation of transmission in the day-ahead time frame, the separation of energy and reserves, the separation of day-ahead unit commitment decisions from real-time dispatch and balancing, and the uncertainty stemming from renewable forecast errors. The market coupling design is compared to two centralized nodal designs: deterministic and stochastic unit commitment.

Our study finds that market design can exert an influence on physical operations, which far exceeds the benefits of stochastic unit commitment relative to deterministic unit commitment. A decentralized zonal market can undermine system performance in two ways: (*i*) by leading to suboptimal commitment of slow generators and creating significant unscheduled flows in day-ahead markets, and (*ii*) by applying suboptimal balancing strategies due to partial coordination among multiple system operators in real time. The first type of problem affects only the European market, where institutional barriers have blocked the implementation of LMPs and the splitting of wide zones into smaller ones. In contrast, the second type of problem currently affects both the continental European system and the wide interconnections in US systems. Moreover, the lack of real-time coordination can harm operational security in extreme situations. This has motivated system operators of both systems to study alternatives for better coordination in balancing, for instance, imbalance netting and the harmonization of balancing products in Europe.

Future extensions of the present work include (*i*) a receding horizon model of real-time operations that represents the influence of ramp rate constraints more accurately, (*ii*) the study of the impact of ramp rate constraints in a finer time scale (e.g. 5 minutes), (*iii*) the representation of resources (e.g. CCGT, hydro and nuclear) in greater detail, and (*iv*) the representation of active transmission network management.

ACKNOWLEDGMENT

The authors would like to thank Pr. (E.) Yves Smeers (UC Louvain), Pr. Matheiu Van Vyve (UC Louvain) and Dr. Andreas Ehrenmann (ENGIE) for their comments and thoughtful discussions during the development of this work.

The authors would also like to thank the Fair Isaac Corporation FICO for providing licenses for Xpress, and the Lawrence Livermore National Laboratory for granting access and computing time at the Sierra cluster.

This research was funded by the ENGIE Chair on Energy Economics and Energy Risk Management and by the Univeristé catholique de Louvain through an FSR grant.

REFERENCES

[1] European Network of Transmission System Operators for Electricity (ENTSO-E), URL: http://www.entsoe.eu/, accessed: 2014-11-09.

[2] European Commission, "Directive 2009/28/EC of the European Parliament and of the Council of 23 April 2009, on the promotion of the use of energy from renewable sources and amending and subsequently repealing Directives 2001/77/EC and 2003/30/EC," 2009.

[3] ——, "COMMUNICATION FROM THE COMMISSION TO THE EUROPEAN PARLIAMENT, THE COUNCIL, THE EUROPEAN ECONOMIC AND SOCIAL COMMITTEE AND THE COMMITTEE OF THE REGIONS, A Roadmap for moving to a competitive low carbon economy in 2050," 2011.

[4] "UMBRELLA Project Final Report," January 2016. [Online]. Available: http://www.e-umbrella.eu/documents

[5] CEPS, PSE, MAVIR, and SPS, "Unplanned flows in the CEE region: In relation to the common market area Germany - Austria," January 2013.

[6] 50Hertz Transmission GmbH, Amprion GmbH, Elia System Operator NV, TenneT TSO B.V., TenneT TSO GmbH, and TransnetBW GmbH, "Potential cross-border balancing cooperation between the Belgian, Dutch and German electricity Transmission System Operators," October 2014, report prepared by the Institute of Power Systems and Power Economics and E-Bridge Consulting GmbH.

[7] APX Group, Belpex, Cegedel Net, EEX, ELIA Group, EnBw, E-On Netz, Powernext, RTE, RWE, and TenneT, "A report for the regulators of the Central West European (CWE) region on the final design of the market coupling solution in the region, by the CWE MC Project," January 2010, (Avalaible at: http://www.epexspot.com/en/market-coupling/documentation_cwe).

[8] A. Ehrenmann and Y. Smeers, "Inefficiencies in European congestion management proposals," *Utilities Policy*, vol. 13, no. 2, pp. 135 – 152, 2005.

[9] PJM, "PJM Manual 11: Energy & Ancillary Services Market Operations," December 2015.

[10] Midcontinent ISO, "Energy and Operating Reserve Markets Business Practice Manual," March 2016.

[11] California ISO, "Business Practice Manual for Market Operations," November 2015.

[12] New York ISO, "Transmission and Dispatching Operations Manual," February 2016.

[13] ——, "Market Administration and Control Area Services Tariff," February 2016.

[14] North American Electric Reliability Corporation (NERC), "Interchange Reference Guidelines," March 2012.

[15] Southwest Power Pool, "Interchange Scheduling Reference Manual," October 2015.

[16] Y. Makarov, R. Diao, P. Etingov, S. Malhara, N. Zhou, R. Guttromson, J. Ma, P. Du, N. Samaan, and C. Sastry, "Analysis methodology for balancing authority cooperation in high penetration of variable generation," Pacific Northwest National Laboratory, Tech. Rep. PNNL-19229, February 2010.

[17] ENTSO-E, "Network Code on Electricity Balancing," August 2014, (Available at: http://networkcodes.entsoe.eu/market-codes/electricity-balancing/).

[18] North American Electric Reliability Corporation (NERC), "Standard BAL-001-1 – Real Power Balancing Control Performance," enforcement date: April 1, 2014.

[19] M. Bjørndal and K. Jrnsten, "Zonal pricing in a deregulated electricity market," *The Energy Journal*, vol. 22, no. 1, pp. 51–73, 2001.

[20] A. H. van der Weijde and B. F. Hobbs, "Locational-based coupling of electricity markets: benefits from coordinating unit commitment and balancing markets," *Journal of Regulatory Economics*, vol. 39, no. 3, pp. 223–251, 2011.

[21] G. Oggioni and Y. Smeers, "Degrees of coordination in market coupling and counter-trading," *The Energy Journal*, vol. 33, no. 3, pp. 39 – 90, 2012.

[22] G. Oggioni, F. Murphy, and Y. Smeers, "Evaluating the impacts of priority dispatch in the European electricity market," *Energy Economics*, vol. 42, pp. 183 – 200, 2014.

[23] F. Leuthold, H. Weigt, and C. von Hirschhausen, "When the wind blows over europe – a simulation analysis and the impact of grid extensions," *Dresden University of Technology, Chair of Energy Economics, Electricity Market Working Paper*, no. WP-EM-31, 2009.

[24] T. Mirbach, S. Ohrem, S. Schild, and A. Moser, "Impact of a significant share of renewable energies on the european power generation system," in *Energy Market (EEM), 2010 7th International Conference on the European*, June 2010, pp. 1–6.

[25] S. Spiecker and C. Weber, "The future of the european electricity system and the impact of fluctuating renewable energy a scenario analysis," *Energy Policy*, vol. 65, pp. 185 – 197, 2014.

[26] KEMA Consulting GmbH, "Impact of a significant share of renewable energies on the european power generation system," European Commission, Tech. Rep. 9011-700, June 2014.

[27] J. Deane, . Driscoll, and B. . Gallachir, "Quantifying the impacts of national renewable electricity ambitions using a northwest european electricity market model," *Renewable Energy*, vol. 80, pp. 604 – 609, 2015.

[28] F. Leuthold, H. Weigt, and C. von Hirschhausen, "Efficient pricing for european electricity networks the theory of nodal pricing applied to

feeding-in wind in germany," *Utilities Policy*, vol. 16, no. 4, pp. 284 – 291, 2008, european Regulatory Perspectives.
[29] R. Barth, J. Apfelbeck, P. Vogel, P. Meibom, and C. Weber, "Load-flow based market coupling with large-scale wind power in Europe," in *Proceedings of the 8th International Workshop on Large Scale Integration of Wind Power into Power Systems as well as on Transmission Networks for Offshore Wind Farms*, Bremen, October 2009, pp. 296–303.
[30] K. Neuhoff, J. Barquin, J. W. Bialek, R. Boyd, C. J. Dent, F. Echavarren, T. Grau, C. von Hirschhausen, B. F. Hobbs, F. Kunz, C. Nabe, G. Papaefthymiou, C. Weber, and H. Weigt, "Renewable electric energy integration: Quantifying the value of design of markets for international transmission capacity," *Energy Economics*, vol. 40, no. 0, pp. 760 – 772, 2013.
[31] J. Abrell and F. Kunz, "Integrating intermittent renewable wind generation - a stochastic multi-market electricity model for the european electricity market," *Networks and Spatial Economics*, vol. 15, no. 1, pp. 117–147, 2015. [Online]. Available: http://dx.doi.org/10.1007/s11067-014-9272-4
[32] A. Tuohy, P. Meibom, E. Denny, and M. O'Malley, "Unit commitment for systems with significant wind penetration," *Power Systems, IEEE Transactions on*, vol. 24, no. 2, pp. 592–601, May 2009.
[33] J. Morales, A. Conejo, and J. Perez-Ruiz, "Economic valuation of reserves in power systems with high penetration of wind power," *Power Systems, IEEE Transactions on*, vol. 24, no. 2, pp. 900–910, May 2009.
[34] A. Papavasiliou and S. S. Oren, "Multiarea stochastic unit commitment for high wind penetration in a transmission constrained network," *Operations Research*, vol. 61, no. 3, pp. 578–592, 2013.
[35] R. Jiang, J. Wang, and Y. Guan, "Robust unit commitment with wind power and pumped storage hydro," *Power Systems, IEEE Transactions on*, vol. 27, no. 2, pp. 800–810, May 2012.
[36] J. Deane, G. Drayton, and B. . Gallachir, "The impact of sub-hourly modelling in power systems with significant levels of renewable generation," *Applied Energy*, vol. 113, pp. 152 – 158, 2014.
[37] H. Gangammanavar, S. Sen, and V. Zavala, "Stochastic optimization of sub-hourly economic dispatch with wind energy," *Power Systems, IEEE Transactions on*, vol. PP, no. 99, pp. 1–11, 2015.
[38] E. Bakirtzis, P. Biskas, D. Labridis, and A. Bakirtzis, "Multiple time resolution unit commitment for short-term operations scheduling under high renewable penetration," *Power Systems, IEEE Transactions on*, vol. 29, no. 1, pp. 149–159, Jan 2014.
[39] EPEX Spot, "EPEX Spot Market Rules and Regulations," URL: http://www.epexspot.com/en/extras/download-center/documentation, September 2015, accessed: 2015-11-24.
[40] EUPHEMIA, "Public Description. PCR Market Coupling algorithm," oct 2013, (Avalaible online: http://static.epexspot.com/document/27917/Euphemia).
[41] ENTSO-E, "Network Code on Load-Frequency Control and Reserves," June 2013, (Available at: http://networkcodes.entsoe.eu/operational-codes/load-frequency-control-reserves/).
[42] Swissgrid Ltd., "Basic principles of acillary service products," February 2015.
[43] Y. Gebrekiros, G. Doorman, S. Jaehnert, and H. Farahmand, "Reserve procurement and transmission capacity reservation in the northern european power market," *International Journal of Electrical Power & Energy Systems*, vol. 67, pp. 546 – 559, 2015.
[44] ELIA Group, "The CIPU contract: a set framework for taking part in the high-voltage grid management," 2008.
[45] Reseau de transport d'électricité (RTE), "Règles Services Système," July 2014.
[46] B. Ernst, C. Scholz, U. Schreier, H. Erbring, F. Berster, S. Schlunke, J. Pease, and Y. Makarov, "Large-scale wind and solar integration in germany," Pacific Northwest National Laboratory, Tech. Rep. PNNL-19225, February 2010.
[47] Union for the Coordination of Transmission of Electricity (UCTE), "UCTE Operation Handbook," 2004, (Available online: https://www.entsoe.eu/publications/system-operations-reports/operation-handbook/Pages/default.aspx).
[48] TenneT, "Determining securely available cross-border transmission capacity," April 2014.
[49] M. Madani and M. Van Vyve, "Computationally efficient MIP formulation and algorithms for european day-ahead electricity market auctions," *European Journal of Operational Research*, vol. 242, no. 2, pp. 580 – 593, 2015.
[50] F. Glover, "Improved linear integer programming formulations of nonlinear integer problems," *Management Science*, vol. 22, no. 4, pp. 455–460, 1975.
[51] F. Leuthold, H. Weigt, and C. von Hirschhausen, "A large-scale spatial optimization model of the european electricity market," *Networks and Spatial Economics*, vol. 12, no. 1, pp. 75–107, 2012.
[52] N. Hutcheon and J. Bialek, "Updated and validated power flow model of the main continental European transmission network," in *2013 IEEE PowerTech Grenoble*, June 2013, pp. 1–5.
[53] J. Egerer, C. Gerbaulet, R. Ihlenburg, F. Kunz, B. Reinhard, C. von Hirschhausen, A. Weber, and J. Weibezahn, *Electricity sector data for policy-relevant modeling: data documentation and applications to the German and European electricity markets*, ser. Data documentation / DIW. Berlin : DIW, 2014, no. 72.
[54] ENTSO-E, "Yearly statistics & adequacy retrospect 2013," 2014, (Available online: http://www.entsoe.eu/publications/statistics/yearly-statistics-and-adequacy-retrospect/).
[55] TenneT, "Quality & capacity plan 2010-2016," 2009, (Available online: http://www.tennet.eu/nl/about-tennet/news-press-publications/publications/technical-publications.html).
[56] C. Davis, A. Chmieliauskas, G. Dijkema, and I. Nikolic, "Enipedia," Energy & Industry group, Faculty of Technology, Policy and Management, TU Delft, Delft, The Netherlands, 2014, (Available online: http://enipedia.tudelft.nl).
[57] Reseau de transport d'électricité (RTE), "Customer's portal & éCO2mix," URLs: http://clients.rte-france.com/index_en.jsp, http://www.rte-france.com/fr/eco2mix/eco2mix/, accessed: 2014-11-28.
[58] ELIA Group, "Elia Grid Data," URL: http://www.elia.be/fr/grid-data/, accessed: 2014-11-09.
[59] European Energy Exchange (EEX), "EEX transparency platform," URL: http://www.transparency.eex.com/, accessed: 2014-11-09.
[60] Austrian Power Grid AG (APG), "Market information," URL: http://www.apg.at/en/market/.
[61] TenneT, "Energieinfo," URL: http://energieinfo.tennet.org/, accessed: 2014-12-10.
[62] H. Heitsch and W. Römisch, "A note on scenario reduction for two-stage stochastic programs," *Operations Research Letters*, vol. 35, no. 6, pp. 731–738, Nov. 2007.
[63] Y. Colombani and S. Heipcke, "Multiple models and parallel solving with Mosel," Dash Optimization, Blisworth House, Blisworth, Northants NN7 3BX, UK, February 2014, avalaible at: http://community.fico.com/docs/DOC-1141. Accessed: 2014-11-20.
[64] I. Aravena and A. Papavasiliou, "A distributed asynchronous algorithm for the two-stage stochastic unit commitment problem," in *2015 IEEE PES General Meeting — Conference Exposition*, July 2015, pp. 1–5, (accepted).
[65] Federal Statistical Office, Germany, "DESTATIS, gross electicity production," URL: https://www.destatis.de/EN/FactsFigures/Economic Sectors/Energy/Production/Tables/GrossElectricityProduction.html, accessed: 2015-11-12.
[66] European Commission, "Eurostat, supply of electicity – monthly data," URL: http://ec.europa.eu/eurostat/, product code: nrg_105m, accessed: 2015-11-12.
[67] J. Han and A. Papavasiliou, "The impacts of transmission topology control on the european electricity network," *IEEE Transactions on Power Systems*, vol. PP, no. 99, pp. 1–12, 2015.

APPENDIX A
NOMENCLATURE

Sets

T_{60}	hourly periods, $T_{60} = \{1, \ldots, 24\}$
T_{15}	15 minute periods, $T_{15} = \{1, \ldots, 96\}$
A	zones
N	buses
L	lines
K	interconnectors
G	thermal generators
$T_{15}(\tau)$	15 minute periods within hour τ
$N(a)$	nodes in zone a
$L(n,m)$	lines between buses n and m, directed from n to m
$L_{\times}(a,b)$	cross-border lines connecting zones a and b, directed from a to b

$K(a,b)$	interconnectors between zones a and b, directed from a to b
Ξ	corners of NTC hyper-rectangle
$G(n)$	thermal generators at node n (or set of nodes n)
$\mathcal{N}_\tau^{NTC}$	set of feasible exchanges with respect to NTCs
$\mathcal{N}_\tau^{OPF}$	set of feasible exchanges with respect to DC OPF
G_{SLOW}	slow generators
G_{FAST}	fast generators
I	continuous bids
J	block bids
$\bar{G}$	exclusive groups
$I(a)$	continuous bids in zone a
$J(a)$	block bids in zone a
$J_E(g)$	block bids within exclusive group g
$\mathcal{D}_g^{60}$	set of feasible generator production decisions for hourly resolution
$\mathcal{D}_g^{15,R}$	set of feasible generator production and reserve decisions for 15-minute resolution
$\mathcal{D}_g^{15}$	set of feasible production decisions for 15-minute resolution

Parameters

$\tau(t)$	corresponding hour of quarter t
$F_l^{\pm}$	flow bounds, line l
B_l	susceptance, line l
$n(l), m(l)$	departing and arrival buses, line l
$D_{n,t}$	demand at bus n on period t
$\bar{\xi}_{n,t}$	forecast renewable supply at bus n, period t
$n_{k,\tau}^{BCE}$	Base Case Exchange through interconnector k in hour τ
R_a^{FCR}	FCR requirement in zone a (similarly defined for aFRR and mFRR)
$TTC_{k,\tau}^{\pm}$	total transfer capacity, interconnector k, hour τ
$NTC_{k,\tau}^{\pm}$	net transfer capacity, interconnector k, hour τ
$ATC_{k,\tau}^{\pm}$	available transfer capacity, interconnector k, hour τ
$a(k), b(k)$	departing and arrival zones, interconnector k
Q_τ^i	quantity offered, bid i, hour τ
P^i	unitary price, bid i
M_j	big-M parameter, block bid j
$\hat{a}(i)$	area of bid i
$C_g(q)$	hourly production cost function, generator g
Q_j^g	discrete output quantities, generator g
C_j^g	discrete production costs, generator g
m_g	number of discrete production bins, generator g
K_g	no load cost, generator g
S_g	startup cost, generator g
$h_g(\boldsymbol{\omega}, \boldsymbol{v})$	total cost of production profile $(\boldsymbol{\omega}, \boldsymbol{v})$, generator g
$\Delta Q_{a,\tau}^{MC}$	day-ahead net position of zone a, hour τ
$u_{g,\tau}^{MC}$	day-ahead preliminary commitment, generator g, hour τ
$u_{g,\tau}^R, v_{g,\tau}^R$	day-ahead definitive commitment and startup, generator g, hour τ
V	value of lost load
CL	day-ahead net position update penalty
$\zeta_{n,s,t}$	renewable supply at bus n, Monte Carlo sample s, period t

Variables

$q_g, q_g^i, q_{g,t}$	quantity produced, generator g
$f_l, f_l^i, f_{l,t}$	flow through line l
$\theta_n, \theta_n^i, \theta_{n,t}$	voltage angle, bus n
x_i	acceptance/rejection continuous bid i
y_j	acceptance/rejection block bid j
$n_{k,\tau}$	exchange through interconnector k, hour τ
$p_{a,\tau}$	energy price in zone a, hour τ
s_i, s_g	surplus of bid i (exclusive group g)
$\lambda_{k,\tau}^{\pm}$	congestion price, interconector k, hour τ
$u_{g,\tau}, v_{g,\tau}$	commitment and startup, generator g, hour τ
$\omega_{j,\tau}^g$	acceptance of production bin j, generator g, hour τ
$r_{g,t}^{FCR}$	FCR provision, generator g, period t (similarly defined for aFRR and mFRR)
$o_{n,t}$	production shedding at bus n, period t
$e_{n,t}$	load shedding at bus n, period t
$\delta_{a,\tau}$	day-ahead net position update, zone a, hour τ

Ignacio Aravena (M'13) obtained his B.Sc. and M.Sc. degrees in Electrical Engineering from Universidad Técnica Federico Santa María (UTFSM), Chile, where he also served as lecturer. He is currently a Ph.D. student on Applied Mathematics at Université Catholique de Louvain (UCL), Belgium.

Anthony Papavasiliou (M'06) received the B.S. degree in electrical and computer engineering from the National Technical University of Athens, Greece, and the Ph.D. degree from the Department of Industrial Engineering and Operations Research (IEOR) at the University of California at Berkeley, Berkeley, CA, USA. He holds the ENGIE Chair at the Université catholique de Louvain, Louvain-la-Neuve, Belgium, and is also a faculty member of the Center for Operations Research and Econometrics. He has served as a consultant for N-SIDE, Pacific Gas and Electric, Quantil and Sun Run and has interned at the Federal Energy Regulatory Commission, the Palo Alto Research Center and the Energy, Economics and Environment Modelling Laboratory at the National Technical University of Athens.